Bijaya K. Nayak,[1] Karthigayan Shanmugasundaram,[1] William E. Friedrichs,[1] Rita C. Cavaglierii,[1] Mandakini Patel,[1] Jeffrey Barnes,[1,2] and Karen Block[1,2]

HIF-1 Mediates Renal Fibrosis in OVE26 Type 1 Diabetic Mice

Diabetes 2016;65:1387–1397 | DOI: 10.2337/db15-0519

Hypoxia-inducible factor (HIF)-1 mediates hypoxia- and chronic kidney disease–induced fibrotic events. Here, we assessed whether HIF-1 blockade attenuates the manifestations of diabetic nephropathy in a type 1 diabetic animal model, OVE26. YC-1 [3-(5′-hydroxymethyl-2′-furyl)-1-benzyl indazole], an HIF-1 inhibitor, reduced whole kidney glomerular hypertrophy, mesangial matrix expansion, extracellular matrix accumulation, and urinary albumin excretion as well as NOX4 protein expression and NADPH-dependent reactive oxygen species production, while blood glucose levels remained unchanged. The role of NOX oxidases in HIF-1–mediated extracellular matrix accumulation was explored in vitro using glomerular mesangial cells. Through a series of genetic silencing and adenoviral overexpression studies, we have defined GLUT1 as a critical downstream target of HIF-1α mediating high glucose–induced matrix expression through the NADPH oxidase isoform, NOX4. Together, our data suggest that pharmacological inhibition of HIF-1 may improve clinical manifestations of diabetic nephropathy.

Diabetic nephropathy (DN) is a major complication of diabetes and is the leading cause of end-stage renal disease. DN is characterized, in part, by glomerular hypertrophy, glomerular and interstitial fibrosis, and the development of albuminuria. High glucose (HG), accumulation of advanced glycation end products (AGEs), oxidative stress, and cytokines such as transforming growth factor-β (TGF-β) are mediators of renal injury in the diabetes environment (1–3). Hypoxia-inducible factors (HIFs) are master transcriptional regulators of genes involved in glucose utilization, cell metabolism, cell survival, angiogenesis, oxidative stress, and fibrogenesis. Several studies have demonstrated a positive role for HIF-1 in mediating renal injury using chronic kidney disease models. For example, *1*) genetic ablation of epithelial HIF-1α inhibited unilateral ureteral obstruction-induced tubulointerstitial fibrosis (4); *2*) in von Hippel–Lindau $(VHL)^{-/-}$ mice, stable expression of HIF-1α promotes interstitial fibrosis (5); and *3*) increased stability of HIF-1α in mice, with podocyte-specific deletion of the von Hippel–Lindau gene, vhlh, alters podocyte survival and metabolism (6). Immunohistochemistry analysis shows enhanced HIF-1α expression in the tubular and glomerular compartment of patients with tubulointerstitial injury with chronic kidney disease and diabetes (4). The expression of HIFs is tightly regulated through transcriptional, translational, and posttranslational mechanisms (7–10). In the presence of oxygen (normoxia), the α-subunits (α) of HIF are hydroxylated and degraded through the 26*S* proteosome by the VHL-E3 ubiquitin ligase complex (7,10). However, in the absence of oxygen (hypoxia), the α-subunits fail to be hydroxylated and escape VHL-dependent degradation. In addition to hypoxia, several nonhypoxic physiological regulators, detected in the diabetes renal environment, participate in the expression and activation of HIF-1 including high levels of glucose (11), angiotensin (Ang) II, protein kinase C (8), TGF-β (9,12,13), reactive oxygen species (ROS) (14,15), and inflammation (16,17). On the other hand, HIF-1 has been implicated in the regulation of the aforementioned physiological drivers of DN (4,9,18,19). Together, these observations suggest a perpetual signaling feedback loop by which HIF-1 mediates the initiation and progression of diabetes-induced renal damage leading ultimately to end-stage renal disease. In the current study, we evaluated the potential renoprotective effects of [3-(5′-hydroxymethyl-2′-furyl)-1-benzyl indazole] (YC-1), an anti–HIF-1 agent in OVE26, a type 1 diabetic mouse model.

[1]Department of Medicine, The University of Texas Health Science Center at San Antonio, San Antonio, TX
[2]Audie L. Murphy Memorial VA Hospital Division, South Texas Veterans Health Care System, San Antonio, TX
Corresponding author: Karen Block, block@uthscsa.edu.

Received 20 February 2015 and accepted 19 January 2016.

B.K.N. and K.S. contributed equally to this work.

RESEARCH DESIGN AND METHODS

Chemicals and Reagents

YC-1 was obtained from Cayman Chemicals.

Experimental Animals and Treatment

OVE26 mice on a friend virus B (FVB) background were used as the experimental model of type 1 diabetes (The Jackson Laboratory, Bar Harbor, ME). FVB mice were used as control. Mice were administered vehicle alone or the HIF-1 inhibitor, YC-1, by oral gavage at ~20 weeks (5 months) of age for 4 weeks. Mice were divided into three groups: group 1, FVB control mice received drug vehicle (1.2% methylcellulose plus 0.1% Polysorbate 80) by oral gavage once a day (n = 7); group 2, OVE26 mice received drug vehicle by gavage once a day (n = 6); and group 3, OVE26 mice received YC-1 (30 mg/kg) by gavage once a day (n = 7). Blood glucose was measured every week on blood samples collected from tail vein in all groups using a glucometer. At the end of the experimental period, animals were weighed and then killed by exsanguination under anesthesia. Both kidneys were removed and weighed; a slice of kidney cortex was embedded in paraffin or flash frozen in liquid nitrogen for microscopy and other experimental (RNA and protein) analyses. All experimental protocols were approved by The University of Texas Health Science Center at San Antonio Institutional Animal Care and Use Committee.

Western Blot Analysis

Kidney cortical lysates were prepared in radioimmune precipitation assay buffer using a Dounce homogenizer. Tissue lysates were rotated for 2 h at 4°C and then centrifuged at 12,000*g* for 15 min at 4°C. After centrifugation, the protein content in the supernatant was measured using the Bradford reagent. For Western blotting, typically 30–50 μg lysate was electrophoresed on an SDS-PAGE and then the separated proteins from gel were electrotransferred on to nitrocellulose membrane. The membrane was blocked with 5% milk in Tris-buffered saline and incubated with primary antibody, HIF-1α, and AGEs (Novus Biologicals, Littleton, CO); fibronectin and actin (Sigma-Aldrich, St. Louis, MO); collagen I and IV and GLUT1 (Abcam, Cambridge, MA); NOX4 (20); and tubulin (Cell Signaling Danvers, MA) at 4°C overnight as per the manufacturers' recommendations. The membrane was washed and then incubated for 1 h with rabbit or mouse horseradish peroxidase–conjugated secondary antibody. The membrane was washed and then developed to visualize protein bands using enhanced chemiluminescence reagent.

Quantitative Real-Time PCR

RNA was extracted from each sample using TRIzol (Invitrogen, Grand Island, NY). cDNA synthesis was carried out with 2 μg total RNA using the cDNA synthesis kit (Qiagen, Valencia, CA). SYBR Green Quantitative Real-Time PCR was performed on 50 ng RNA using the SuperArray kit (SuperArray Biosciences, Valencia, CA) and the Eppendorf RealPlex machine. Primers for mouse fibronectin, collagen I, GLUT1, plasminogen activator inhibitor (PAI)-1, NOX4, and GAPDH were designed as previously described (4,5). Reactions were done in triplicate and normalized to GAPDH.

NADPH Oxidase Assay

NADPH-dependent superoxide generation was measured using a lucigenin-enhanced chemiluminescence method as previously described (20,21).

Histopathological and Urine Albumin Excretion Analysis

Morphometric studies were carried out as previously described (21). Briefly, kidneys were fixed in 10% neutral buffered formalin embedded in paraffin and 5-μm sections were stained with hematoxylin-eosin (H-E) or periodic acid Schiff (PAS). Images were obtained by analyzing a minimum of 25 glomerular sections from each animal with an Axio Imager A1 microscope (Carl Zeiss, Melville, NY). Glomerular tuft area and mesangial matrix expansion were evaluated using the Image-Pro Plus software. Before the sacrifice, mice were placed in metabolic cages and 24-h urines were collected for albumin measurements. Urine albumin was measured using a mouse albumin ELISA quantification set (Bethyl Laboratories, Montgomery, TX) and expressed as milligrams of albumin per 24 h.

Mesangial Cell Transfections and Adenoviral Infections

Mesangial cells (MCs) were transfected using the Amaxa system and subsequently exposed to low glucose plus mannitol osmotic control (LG) or HG. For adenoviral infection experiments, indicated samples were infected with GFP or NOX4 adenovirus for ~8–20 h before harvesting.

Immunofluorescence/Microscopy

The 6-μm thick frozen sections were mounted on glass slides and then fixed in cold acetone. Sections were rehydrated in PBS–0.1% BSA before blocking with the appropriate IgG. The primary antibody, rabbit polyclonal anti–collagen IV, was incubated on the tissue for 1 h at room temperature. Sections were then washed three times for 5 min in PBS–0.1% BSA. Fluorescence-conjugated secondary antibodies, Alexa Fluor 488 (Invitrogen), were added at dilutions of 1:100 for 45 min at room temperature followed by washing in PBS–0.1% BSA. Sections were mounted with ProLong Gold reagent with DAPI (Invitrogen, Grand Island, NY) and allowed to dry before viewing with an Olympus AX70 (Olympus, Melville, NY) microscope equipped for epifluorescence. Images were taken using an Olympus DP70 digital camera.

Immunohistochemistry

Fibronectin expression was analyzed by immunohistochemistry in tissue sections collected from FVB, OVE26, and OVE26+YC-1 mice using polyclonal fibronectin antibodies (1:800; Sigma-Aldrich) as previously described (21). Bound antibody was identified by immunoperoxidase ABC staining following the manufacturer's instructions (Vector

Laboratories, Burlingame, CA). The sections were then dehydrated and mounted with Permount (Sigma-Aldrich) and viewed by bright-field microscopy and photographed as described above.

Statistical Analysis

Results are expressed as the mean ± SEM. Statistical analyses were performed using ANOVA followed by a Fisher test. A P value of 0.05 was used to define statistical significance.

RESULTS

Effects of YC-1 Treatment on Known HIF-1 Target Genes in the Kidney

To examine the effects of HIF-1 inhibition in complications of diabetic kidney disease, we delivered YC-1, a specific HIF-1 inhibitor, to 5-month old OVE26 mice for 4 weeks. YC-1 acts by reducing HIF-1α expression (22). To confirm that YC-1 was successfully delivered to the kidney of OVE26 mice, we evaluated HIF-1α expression levels and mRNA expression of representative HIF-1α target genes. HIF-1α expression was examined in FVB, OVE26, and OVE26+YC-1–treated mice using immunohistochemistry. We found HIF-1α expression to be increased in the glomeruli (arrows) as well as in renal tubular cells of OVE26 mice compared with FVB control as examined by immunohistochemistry. Importantly, HIF-1α expression was reduced with YC-1 treatment (Fig. 1*A*). Western blot analysis confirmed HIF-1α upregulation in OVE26 diabetic mice compared with FVB control, which was significantly reduced in OVE26 mice receiving YC-1 (Fig. 1*B*, left panel). This observation was also noted with GLUT1, a bona fide transcriptional target of HIF-1α (Fig. 1*B*, left panel). Actin was used as a loading control. Quantitation of HIF-1α and GLUT1 expression is included (Fig. 1*B*, right panels). As an independent control, we examined the mRNA of specific HIF-1α target genes. We found that GLUT1 and PAI-1 mRNA expression is significantly higher in OVE26 mice compared with FVB control, whereas OVE26 mice receiving YC-1 exhibited marked reduction of both GLUT1 and PAI-1 mRNA expression, respectively,

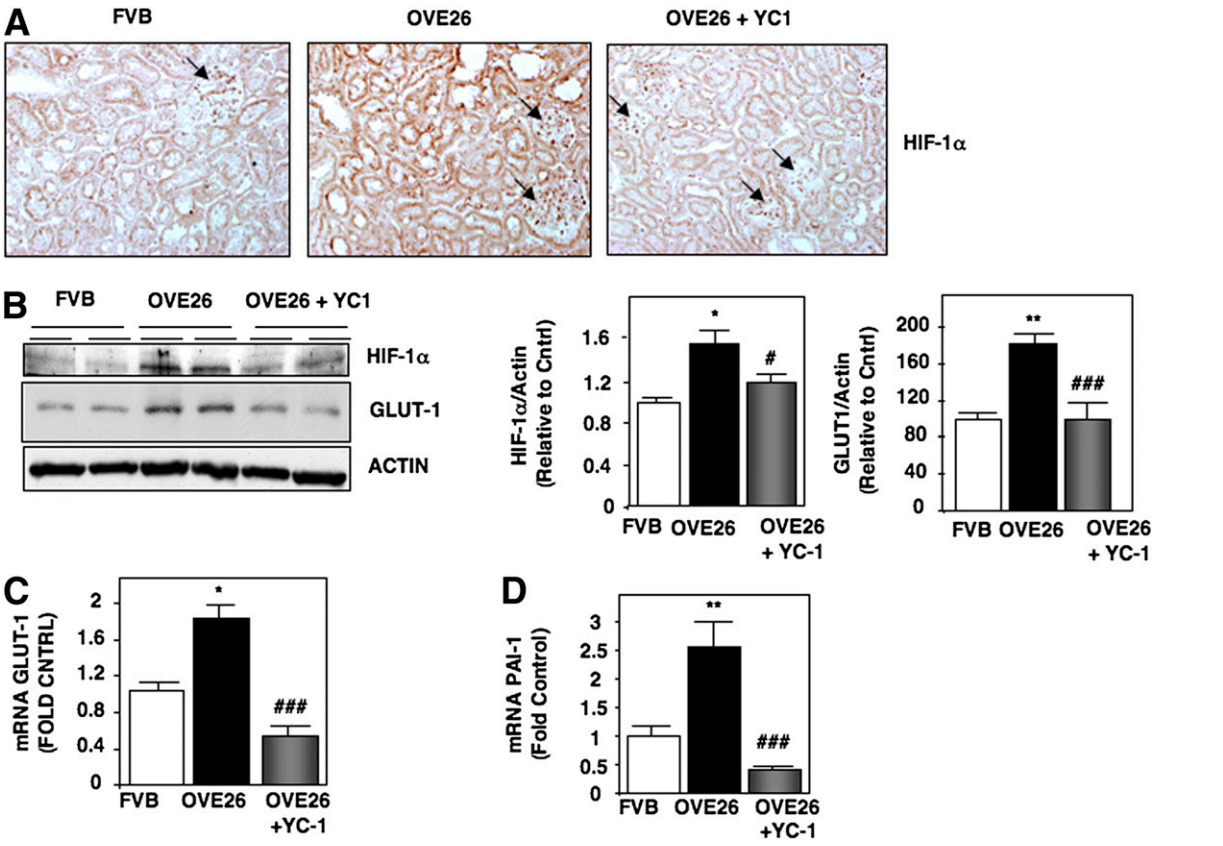

Figure 1—Effects of YC-1 on HIF-1α expression and HIF-1α transcriptional gene targets. *A*: Representative kidney sections of HIF-1α expression detected by immunoperoxidase in FVB control, OVE26 diabetic, and OVE26+YC-1 diabetic mice. Glomeruli are highlighted by arrows. *B*: Expression of HIF-1α was assessed by Western blot analysis from cortical lysates prepared from FVB, OVE26, and OVE26+YC-1 mice. Actin was immunoblotted as a loading control. The histograms represent mean ± SEM from individual mice from each group. Quantitative RT-PCR was performed as outlined in RESEARCH DESIGN AND METHODS to examine the mRNA expression levels of GLUT1 (*C*) and PAI-1 (*D*). The data are representative of three independent experiments and are expressed as fold control where the ratio of the FVB control was defined as 1. Values represent mean ± SEM. *P < 0.05 vs. FVB; **P < 0.01 vs. FVB; #P < 0.05 vs. OVE26; ###P < 0.001 vs. OVE26. Cntrl, control.

compared with OVE26 (Fig. 1*C* and *D*, respectively). Together, these findings suggest that YC-1 was successfully delivered to the renal compartment in OVE26 mice.

Effects of YC-1 Treatment on Blood Glucose, Kidney Weight, Body Weight, and Urine Albumin

OVE26 mice carry a transgene overexpressing calmodulin in pancreatic β-cells resulting in spontaneous high levels of glucose at birth, which reach levels of 600 mg/dL at 2 months of age and continue through the life of the animal (23). OVE26 mice present characteristics (proteinuria, glomerular hypertrophy, glomerular and interstitial fibrosis, and decline in renal function) that mimic human diabetes and its complications at 4–6 months (23,24).

OVE26 mice receiving vehicle alone were used as the diabetic control and FVB as a genetic match nondiabetic control. Table 1 outlines metabolic parameters measured in the three animal groups: FVB, OVE26, and OVE26+YC-1. Blood glucose was significantly higher in the OVE26 mice (567 ± 14 mg/dL) compared with the FVB control (151 ± 22 mg/dL). Delivery of YC-1 did not alter blood glucose (565 ± 27 mg/dL) compared with OVE26 mice receiving vehicle control. Similarly, diabetic OVE26 mice displayed a significant reduction in body weight (18 ± 2.4 g) compared with FVB nondiabetic control (29 ± 3.6 g), which was not significantly altered by the delivery of YC-1. However, whole kidney weight was reduced in YC-1–treated animals (21 ± 0.02 g) compared with OVE26 alone (25 ± 0.03 g), which trended higher than FVB control (23 ± 0.03 g). Examination of kidney weight–to–body weight ratio, an indicator of renal hypertrophy, showed significant increase in OVE26 mice (14.3 ± 0.85 g/kg) compared with FVB control (8.04 ± 0.87 g/kg), while delivery of YC-1 significantly reduced kidney weight–to–body weight ratio from that of OVE26 (12.4 ± 0.84 g/kg). Urine albumin was collected as a general readout of renal injury. Marked increase of albumin levels was detected in the urine of OVE26 mice (14.5 ± 0.3.5 mg) compared with FVB control (0.0914 ± 0.053 mg) collected over a 24-h period, consistent with previous reports (24). Interestingly, urine albumin excretion was significantly reduced in OVE26 mice receiving YC-1 (5.12 ± 0.3.44 mg) compared with OVE26 alone.

Effects of YC-1 Treatment on Diabetes-Induced Glomerular Hypertrophy and Mesangial Matrix Expansion

OVE26 mice on an FVB background are a solid model to evaluate the manifestations of DN (25). Morphological changes in OVE26 kidney have been carefully documented in the context of renal histopathology (glomerular volume, mesangial fraction, and mesangial volume are greatest between ~3 and 6 months of age, and fibrosis is evident and marked at ~5–9 months of age, which is associated with reduced glomerular filtration rate) (24). Together, we chose to evaluate the effects of YC-1 on DN in OVE26 mice between the ages of 5 and 6 months. We examined glomerular hypertrophy in H-E–stained histological sections of kidneys from FVB control, OVE26 diabetic, and OVE26+YC-1–treated mice by measuring glomerular surface area using image analysis. We found that the glomerular surface area is significantly increased in OVE26 mice compared with FVB control mice, which was reduced in OVE26 mice with YC-1 treatment (Fig. 2*A*, left panel). This was confirmed by semiquantitation using the Image-Pro Plus software (Fig. 2*A*, right panel). Mesangial matrix expansion was examined by subjecting sections of paraffin-embedded kidneys to PAS staining. OVE26 mice exhibited marked mesangial expansion compared with FVB control, which was reduced in OVE26 mice that received YC-1 (Fig. 2*B*, left panel) and quantitated (Fig. 2*B*, right panel). Together, our data demonstrate that YC-1 treatment reduces glomerular hypertrophy in type 1 OVE26 diabetic mice.

We examined distribution of extracellular matrix proteins, fibronectin, and collagen IV in renal glomeruli using immunohistochemistry and immunofluorescence, respectively. We find enhanced staining of fibronectin and collagen IV in the glomeruli of OVE26 mice compared with FVB control, which were reduced in OVE26 mice receiving YC-1 (Fig. 2*C* and *D*, respectively, left panels). Quantitation is shown (Fig. 2*C* and *D*, right panels). Fibronectin and collagen I expression was examined in parallel by Western blot analysis using whole kidney cortex. Figure 3*A* shows increased fibronectin and collagen I expression in OVE26 mice compared with FVB control, which was reduced in OVE26 mice with YC-1 treatment. Quantitation is shown (Fig. 3*B* and *C*, respectively).

Table 1—Effects of YC-1 on blood glucose, body weight, kidney weight, kidney weight–to–body weight ratio, and urine albumin levels in OVE26 mice

Parameter	FVB (7)	OVE26 (6)	OVE26+YC-1 (7)
Blood glucose (mg/dL)	151 ± 22	567 ± 14***	565 ± 27***
Body weight (g)	29 ± 3.6	18 ± 2.4***	17 ± 1.5***
Kidney weight (g)	0.23 ± 0.03	0.25 ± 0.03	0.21 ± 0.02**
Kidney weight–to–body weight ratio (g)	8.04 ± 0.87	14.3 ± 0.85***	12.4 ± 0.84*#
Urine albumin (mg/24 h)	0.0914 ± 0.053	14.5 ± 0.3.5***	5.12 ± 3.44**##

Data are mean ± SEM for each group. The numbers in parentheses indicate the number of animals in that group. Glucose level, body weight, kidney weight, kidney weight–to–body weight ratio, and urine albumin measurements after 5 months of diabetes plus 3-week treatment with YC-1. *#$P < 0.05$ vs. OVE26. **##$P < 0.01$ vs. OVE26. **$P < 0.01$ vs. OVE26. ***$P < 0.001$ vs. FVB.

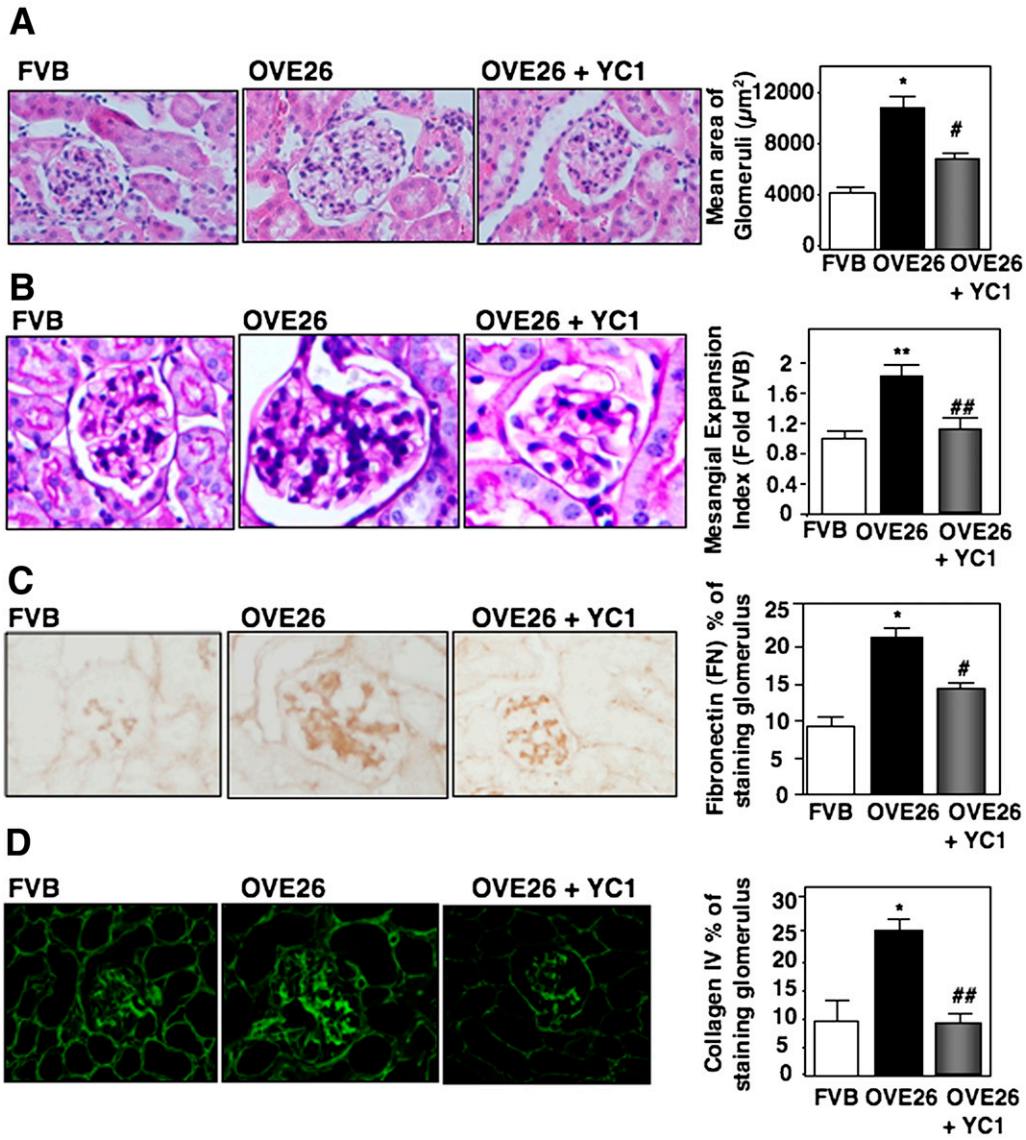

Figure 2—Effects of YC-1 on renal histopathology. *A*: Representative photomicrographs of kidney sections stained with H-E in FVB, OVE26, and OVE26+YC-1 mice. *B*: Representative PAS from FVB, OVE26, and OVE26+YC-1 groups. Representative kidney sections of fibronectin expression detected by immunoperoxidase (*C*) and collagen type IV expression detected by immunofluorescence (*D*) in FVB, OVE26, and OVE26+YC-1 mice. Glomerular cross-sectional areas were measured from kidney sections stained with H-E using the Image-Pro Plus 4.5 software. The histograms represent mean ± SE from 25 individual glomeruli in sections from individual mice from each group. **P* < 0.05 vs. FVB; ***P* < 0.01 vs. FVB; #*P* < 0.05 vs. OVE26; ##*P* < 0.01 vs. OVE26.

Additionally, we found that fibronectin and collagen I mRNA were increased in OVE26 mice compared with FVB control and were significantly reduced in YC-1–treated OVE26 mice (Fig. 3*D* and *E*, respectively).

Effects of YC-1 Treatment on Diabetes-Induced NOX4 Expression and Oxidative Stress in the Kidney

We and others have demonstrated that enhanced oxidative stress, mediated by the NADPH oxidase isoform, NOX4, mediates DN and renal injury (20,21,26,27). For examination of the effects of HIF-1 inhibition on NOX-mediated oxidative stress, NOX4 protein expression and NADPH-dependent superoxide generation were examined in kidney cortex. Western blot analysis showed that NOX4 protein expression was increased in OVE26 mice compared with the FVB control mice, which was reduced in the OVE26 mice with YC-1 treatment (Fig. 4*A*, left and quantitated in right panel). Changes in NOX4 expression correlated with NADPH-dependent superoxide generation (20–27) (Fig. 4*B*). NOX4 harbors hypoxia responsive elements, which are targeted by HIF-1 under hypoxic conditions (19). As we found that YC-1 reduces NOX4 expression, we examined whether this was due to reduced NOX4 gene expression. We found that NOX4 mRNA expression is higher in OVE26 compared with FVB control; interestingly, NOX4 mRNA expression was not affected by

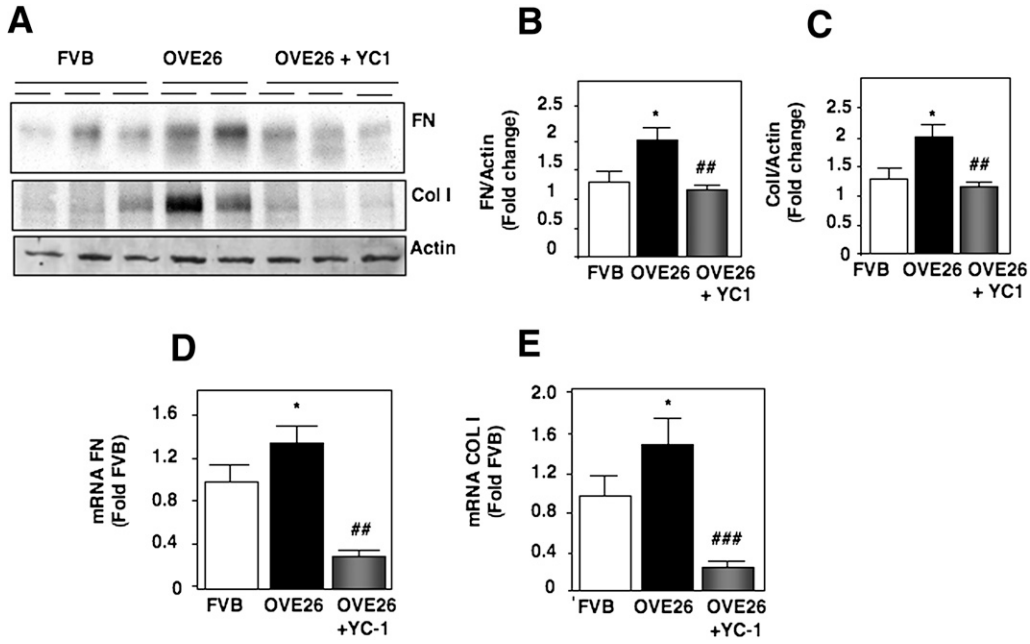

Figure 3—Effects of YC-1 on diabetes-induced extracellular matrix expression. *A*: Expression of fibronectin (FN), collagen type I (COL I), and HIF-1α was assessed by Western blot analysis from cortical lysates prepared from FVB, OVE26, and OVE26+YC-1 mice. Actin was immunoblotted as a loading control. The histograms represent mean ± SEM from 3–6 individual mice from each group. **P* < 0.05 vs. FVB, ##*P* < 0.01 vs. OVE26 for fibronectin (*B*) and collagen I (*C*). Quantitative RT-PCR was performed to examine the mRNA expression levels of fibronectin (*D*) and collagen type I (*E*) in FVB, OVE26, and OVE26+YC-1 mice. The data are representative of three independent experiments and are expressed as fold control where the ratio of the FVB control was defined as 1. Values represent mean ± SEM. **P* < 0.05 vs. FVB; ##*P* < 0.05 vs. OVE26; ###*P* < 0.001 vs. OVE26.

YC-1 treatment in OVE26 animals (Fig. 4*C*). Formation of AGEs is mediated by oxidative stress, which accumulates in the diabetic kidney and contributes to DN (28). We examined AGEs as a biological readout of oxidative stress in FVB, OVE26, and OVE26+YC-1 cortical homogenates. We found enhanced AGEs in OVE26 mice compared with FVB control and, importantly, found that YC-1 reduced AGEs back to levels similar to those in FVB nondiabetic control as examined by Western blot analysis (Fig. 4*D*, left panel). Quantitation of AGEs is shown (Fig. 4*D*, right panel). These data indicate that the HIF-1 inhibitor, YC-1, reduces diabetes-induced NOX4 expression and oxidative stress.

Fibronectin Expression Is Driven by HIF-1 and GLUT1 in MCs

HIF-1 is a recognized transcriptional regulator of glucose receptors. Our in vivo data suggest that GLUT1 may be a critical downstream target of HIF-1, which drives extracellular matrix expression and glomerular hypertrophy in diabetic OVE26 mice. For determination of the role of GLUT1 and definition of the putative mechanisms, we exposed MCs to LG or HG. RNA was extracted and HIF-1α and GLUT1 mRNA expression was examined by quantitative real-time PCR. We found that HG enhanced both HIF-1α and GLUT1 mRNA expression in MCs compared with LG (Fig. 5*A*). To determine the role of HIF-1α and GLUT1 in HG-induced fibronectin expression, we silenced HIF-1α and GLUT1 using small interfering (si)RNA-mediated knockdown. MCs were transfected with scrambled control, siRNA HIF-1α, or GLUT1 as outlined in RESEARCH DESIGN AND METHODS and exposed to LG or HG. Western blot analysis showed that fibronectin expression was higher in MCs transfected with scrambled control exposed to HG compared with LG, while fibronectin expression was markedly reduced in MCs exposed to HG transfected with siHIF-1α (Fig. 5*B*) or siGLUT1 (Fig. 5*C*). Successful knockdown of HIF-1α and GLUT1 was shown (Fig. 5*B* and *C*, respectively).

NOX4 Expression and Activity Are Regulated by GLUT1

Glucose receptors facilitate the transport of glucose from the extracellular milieu to the intracellular compartment in the diabetic kidney (29–32). Enhanced glucose uptake stimulates intracellular oxidative stress. However, the role of GLUT1 as an upstream regulator of NOX4 has not been studied. We examined the effects of GLUT1 silencing on NOX4 expression and activity. MCs were transfected with siRNA GLUT1 or scrambled control. Subsequently, the cells were exposed to LG or HG. Western blot analysis showed, in support of our previous findings, that NOX4 expression was higher in MCs exposed to HG compared with LG (20,21) (Fig. 6*A*). In parallel, NADPH-dependent superoxide production was examined using enhanced chemiluminescence. We found NADPH-dependent superoxide generation to be markedly higher in MCs exposed to HG compared with LG, which was reduced when GLUT1

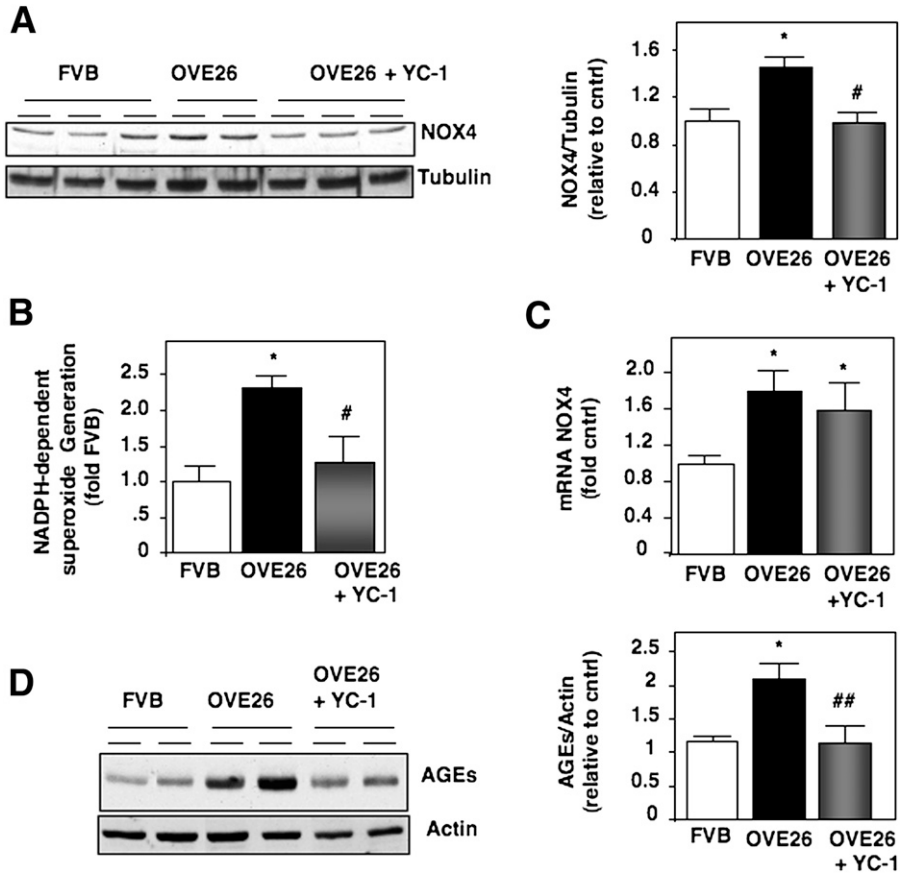

Figure 4—Effects of YC-1 on diabetes-induced oxidative stress. *A*: NOX4 protein expression was assessed by Western blot analysis from cortical lysates prepared from FVB, OVE26, and OVE26+YC-1 mice. Tubulin was immunoblotted as a loading control. *B*: NADPH-dependent superoxide production was examined in cortical homogenates prepared from FVB, OVE26, and OVE26+YC-1 mice as outlined in RESEARCH DESIGN AND METHODS. *C*: Quantitative RT-PCR was performed as outlined in RESEARCH DESIGN AND METHODS to examine the mRNA expression levels of NOX4 in FVB, OVE26, and OVE26+YC-1 mice. The data are representative of three independent experiments and are expressed as fold control where the ratio of the FVB control was defined as 1. *D*: Expression of AGEs was evaluated by Western blot using cortical lysates prepared from FVB, OVE26, and OVE26+YC-1 mice. The histograms represent mean ± SEM from individual mice from each group. *$P < 0.05$ vs. FVB. #$P < 0.05$ vs. OVE26. ##$P < 0.01$ vs. OVE26. cntrl, control.

was silenced (Fig. 6*B*). Together, this suggests that glucose uptake through GLUT1 is a putative mechanism of NOX4 expression regulation and glucose-induced NOX-derived ROS in MCs.

HIF-1α and GLUT1 Mediate Fibronectin Expression Through NOX4

To determine whether HIF-1α and GLUT1 mediate HG-induced fibronectin expression through NOX4, we transfected MCs with scrambled control, siHIF-1α, or siGLUT1 in the presence of HG or LG. Subsequently, we exogenously overexpressed NOX4 using adenovirus or GFP adenovirus control as described in RESEARCH DESIGN AND METHODS. Fibronectin was examined using two independent approaches: Western blot analysis and immunofluorescence. As previously demonstrated, we found that siRNA-mediated knockdown of HIF-1α or GLUT1 reduces HG-induced fibronectin expression (Fig. 7*A–C*), which was not affected by infection of adenovirus GFP (Fig. 7*A–C*). However, adenoviral overexpression of NOX4 overrides these effects where we find fibronectin expression remains high in siRNA-transfected HIF-1α and GLUT1 infected with adenovirus NOX4 compared with adenovirus GFP alone in MCs exposed to HG (Fig. 7*A–C*). NOX4 overexpression was verified (Fig. 7*D*).

DISCUSSION

Here, we provide strong evidence that HIF-1 mediates diabetes-induced renal injury in vivo. This is supported by our findings that YC-1, an anti–HIF-1 agent, reduces renal hypertrophy, extracellular matrix protein accumulation, oxidative stress, and urine albumin excretion in type 1 diabetic OVE26 mice. The significance of this work is highlighted by the finding that HIF-1α expression is detected in archival biopsy tissues from patients with DN and in the kidneys of animal models with type 1 and type 2 diabetes (4,11,33). YC-1 has been similarly used to define positive and negative roles for HIF-1 in human pathologies such as carcinogenesis, coronary ischemic and inflammatory diseases, and hypoxia-induced renal fibrosis (2,5,10,34,35). Studies demonstrate that HIF-1 promotes

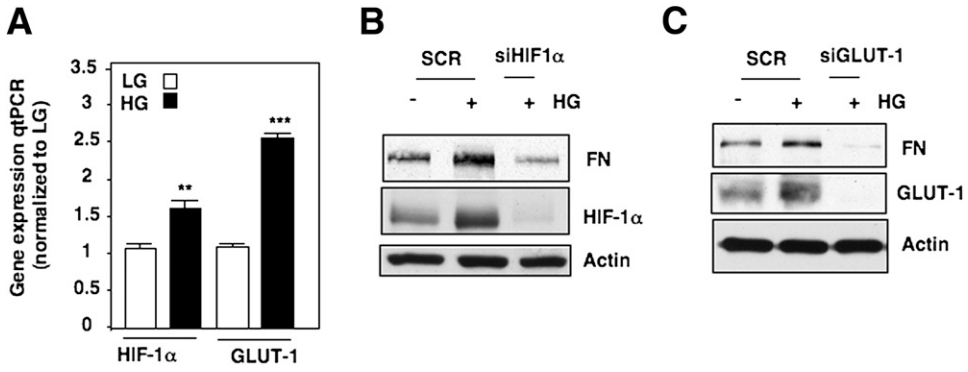

Figure 5—Effects of HIF-1α or GLUT1 knockdown on HG-induced fibronectin expression. *A*: MCs were exposed to LG or HG (HG for 24 h). RNA was extracted and HIF-1α and GLUT1 mRNA were examined by quantitative real-time PCR (qtPCR). MCs were transfected with scrambled control (SCR) or siHIF-1α (*B*) or siGLUT1 (*C*). Expression of fibronectin (FN), HIF-1α, and GLUT1 was evaluated by Western blot. The data are representative of three independent experiments and are expressed as fold control (LG), defined as 1. Values represent mean ± SEM. $^{**}P < 0.01$ vs. HIF-1α LG. $^{***}P < 0.001$ vs. GLUT1 LG.

renal fibrogenesis in mouse models of chronic/hypoxic renal injury models. While genetic ablation of HIF-1α in renal epithelial cells reduces collagen deposition and overall unilateral ureteral obstruction-induced renal fibrosis (4), stable expression of HIF-1α, via VHL deletion, promotes 5/6 ablation-induced tubulointerstitial fibrosis, which is blocked by YC-1 treatment (5). Moreover, glomerulosclerosis and podocyte apoptosis are enhanced in HIF-1α–overexpressing podocytes (6). Albuminuria is evident in OVE26 mice at an early age of 2 months and increases with age (23,24). Compared with FVB control, we found enhanced urine albumin excretion in OVE26 mice concomitant with reduced synaptopodin expression, a component of the foot process cytoskeleton, which is reduced during the course of DN (data not shown). Additionally, we show that delivery of YC-1 significantly reduces albumin excretion in OVE26 mice. However, we did not detect any changes of synaptopodin expression in YC-1 treated OVE26 mice compared with the OVE26 mice alone (data not shown). We did not evaluate podocyte apoptosis in our animal groups. The role of HIF-1 in diabetes-induced podocyte injury remains unclear but is currently under investigation.

In the context of DN, indirect approaches have similarly implicated HIF-1 as a protector or mediator of DN. While Matoba et al. (33) show that rho-kinase blockade attenuates HIF-1α accumulation and renal fibrosis in db/db mice, Nordquist et al. (36) showed that cobalt chloride–dependent stabilization of HIF-1α protects against streptozocin-induced DN in rats. Our findings strongly support a role for HIF-1 as a mediator of glomerular hypertrophy and matrix expansion in DN. It should be noted that our group found that cobalt chloride is an inhibitor of NOX oxidase activity (data not shown), a major mediator of diabetes-induced nephropathy (20,21,26,37–39). Although the mechanisms by which cobalt chloride inhibits NOX activity is unknown, we propose that it is likely due to the fact that cobalt chloride is an iron chelator, an important cofactor required for NOX oxidase activation (40). Alternatively, the differences in findings may be attributed to the diversities of animal models used in the two independent studies.

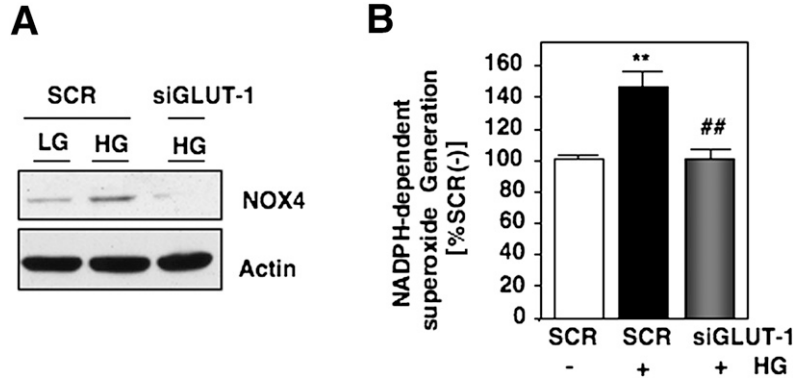

Figure 6—GLUT1 silencing reduces HG-induced oxidative stress. *A*: MCs were transfected with scrambled control (SCR) or siRNA GLUT1. *B*: In parallel experiments, NADPH-dependent superoxide production was examined. The histograms represent mean ± SEM from scrambled control without HG [SCR(-)]. $^{**}P < 0.01$ vs. SCR; $^{\#\#}P < 0.01$ vs. scrambled control plus HG (+).

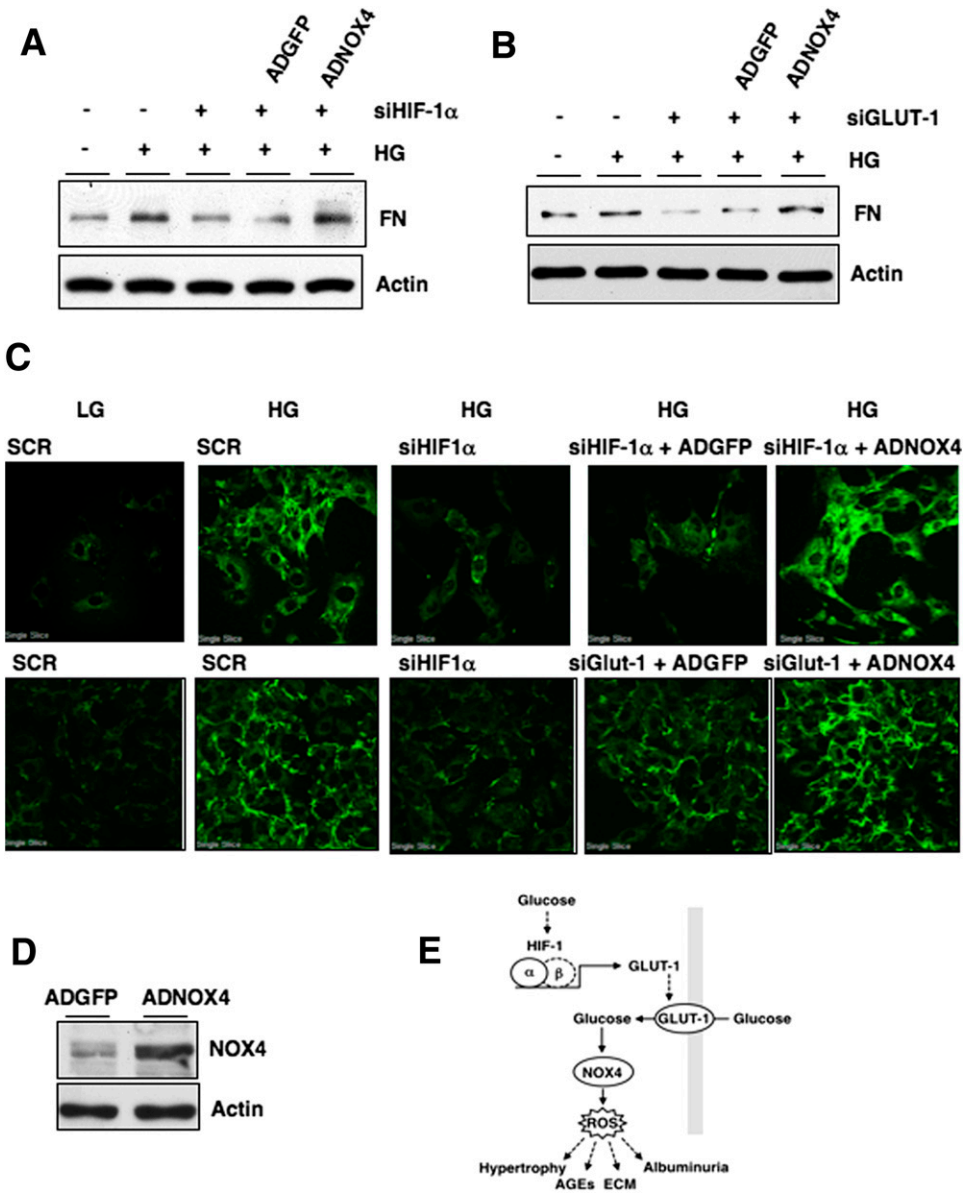

Figure 7—GLUT1 mediates fibronectin expression through NOX4. MCs were transfected and exposed to LG or HG 7. Before harvesting, indicated plates were infected with adenovirus GFP (ADGFP) or adenovirus NOX4 (ADNOX4). *A* and *B*: Fibronectin (FN) expression was assessed by Western blot analysis. Actin was immunoblotted as a loading control. *C*: Parallel to *A* and *B*, cells were plated on cover slips. Fibronectin was examined by immunofluorescence as outlined in RESEARCH DESIGN AND METHODS. *D*: NOX4 expression was assessed in MCs infected with adenovirus GFP or adenovirus NOX4. *E*: Schematic for HIF-1 inhibition blocking progression of DN through reduction of GLUT1-dependent, NOX4-derived oxidative stress in vitro and in vivo. ECM, extracellular matrix; SCR, scrambled control.

DN is driven by exposure of the kidney to complex microenvironmental factors that are known to stabilize HIF-1α including excess levels of glucose (11), TGF-β (13), AngII (10), and tissue hypoxia (4). The aforementioned factors mediate initiation and progression of diabetes-induced glomerular and tubulointerstitial injury, in part, through induction of oxidative stress, activation of intracellular signaling pathways, and upregulation of genes that promote fibrogenesis. Importantly, HIF-1 is also noted to transcriptionally regulate genes of key proteins that generate oxidative stress (19) and mediate glucose (7) and matrix metabolism (4), suggesting that positive-feedback loops and cross talks between pathways exist and are involved. Our findings that diabetes-mediated mesangial expansion and extracellular matrix protein synthesis as well as NOX4 expression and ROS production are attenuated in OVE26 mice treated with YC-1 support the concept that HIF-1 is deleterious in the diabetic environment.

HIF-1 promotes tubulointerstitial fibrosis, in part, through upregulation of the extracellular matrix-modifying factor PAI-1 (4). In support of this, we found that PAI-1 gene expression is upregulated in OVE26 diabetic mice compared with FVB control, which is significantly reduced in YC-1–treated animals concomitant with reduced

fibronectin, collagen I, and collagen IV. YC-1 treatment in OVE26 mice resulted in hyperreduction of fibronectin and collagen 1 mRNA, whereas the protein expression of the aforementioned genes was reduced to near basal levels, together suggesting that direct and indirect posttranscriptional and/or posttranslational events are additionally involved in the regulation of the aforementioned proteins. Importantly, we found that another bona fide HIF-1 gene target, GLUT1, was similarly increased in diabetic OVE26 mice and was significantly reduced in YC-1–treated animals. In the kidney, GLUT1 is constitutively expressed in both the glomerular and tubular compartments and promotes hyperglycemia-induced renal injury (41–43). Renal glomerular MCs upregulate GLUT1 to enhance glucose uptake in response to diabetes, which is an important inducer of extracellular matrix formation and deposition as well as formation of AGEs (28–30,41,44). Our data, presented herein, suggest that HIF-1 mediates extracellular matrix accumulation, renal hypertrophy, and AGE formation through mechanisms involving increased glucose uptake with subsequent activation of NOX4 (Fig. 7*E*). This is supported by our findings that NOX4 expression and NADPH-dependent superoxide generation are higher in OVE26 mice compared with FVB control and reduced in the OVE26 animals with YC-1 treatment. NOX4 has been termed an oxygen sensor and is a transcriptional target of HIF-1 (19). Interestingly, we found that NOX4 mRNA levels were increased in the kidneys of OVE26 diabetic mice compared with FVB control, whereas delivery of YC-1 did not reduce NOX4 mRNA. Although our group has demonstrated that high levels of glucose promote NOX4-mediated glomerular injury in streptozocin-induced models of type 1 diabetes in rat via increased NOX4 expression and NOX4-dependent ROS generation, the molecular mechanisms by which hyperglycemia exerts its actions remain unclear. Through a series of genetic silencing and adenoviral overexpression studies, we have defined GLUT1 as a critical target of HIF-1α in HG-induced NOX4 expression and activation and extracellular matrix accumulation in MCs and in the diabetic kidney (20,21).

In conclusion, the issue of elucidating the role and defining the mechanisms by which HIF-1 mediates initiation and progression of DN is in its infancy but is critical to determine whether HIF-1 is a potential therapeutic target for the treatment of DN.

Acknowledgments. This article is dedicated to the memory of the authors' friend and colleague, Dr. Hanna E. Abboud. The authors thank Drs. Hanna E. Abboud, Yves Gorin, and Denis Feliers for critical reading of the manuscript.

Funding. This work was supported by the U.S. Department of Veterans Affairs Merit Award (grant to K.B.), a multi-project grant from JDRF (to K.B.), and the National Institute of Diabetes and Digestive and Kidney Diseases (DK-033665 to K.B.).

Duality of Interest. No potential conflicts of interest relevant to this article were reported.

Author Contributions. B.K.N. and K.S. contributed to the generation of research data. W.E.F. contributed to animal experiments. R.C.C. and J.B. contributed to morphometric analysis and staining and data interpretation. M.P. amplified adenoviruses. K.B. designed experiments, contributed to the generation of research data, analyzed the data, and wrote the manuscript. K.B. is the guarantor of this work and, as such, had full access to all the data in the study and takes responsibility for the integrity of the data and the accuracy of the data analysis.

References

1. Singh DK, Winocour P, Farrington K. Mechanisms of disease: the hypoxic tubular hypothesis of diabetic nephropathy. Nat Clin Pract Nephrol 2008;4:216–226
2. Dronavalli S, Duka I, Bakris GL. The pathogenesis of diabetic nephropathy. Nat Clin Pract Endocrinol Metab 2008;4:444–452
3. Kanwar YS, Sun L, Xie P, Liu FY, Chen S. A glimpse of various pathogenetic mechanisms of diabetic nephropathy. Annu Rev Pathol 2011;6:395–423
4. Higgins DF, Kimura K, Bernhardt WM, et al. Hypoxia promotes fibrogenesis in vivo via HIF-1 stimulation of epithelial-to-mesenchymal transition. J Clin Invest 2007;117:3810–3820
5. Kimura K, Iwano M, Higgins DF, et al. Stable expression of HIF-1alpha in tubular epithelial cells promotes interstitial fibrosis. Am J Physiol Renal Physiol 2008;295:F1023–F1029
6. Brukamp K, Jim B, Moeller MJ, Haase VH. Hypoxia and podocyte-specific Vhlh deletion confer risk of glomerular disease. Am J Physiol Renal Physiol 2007; 293:F1397–F1407
7. Maxwell PH, Wiesener MS, Chang GW, et al. The tumour suppressor protein VHL targets hypoxia-inducible factors for oxygen-dependent proteolysis. Nature 1999;399:271–275
8. Pagé EL, Robitaille GA, Pouysségur J, Richard DE. Induction of hypoxia-inducible factor-1alpha by transcriptional and translational mechanisms. J Biol Chem 2002;277:48403–48409
9. Semenza GL. Targeting HIF-1 for cancer therapy. Nat Rev Cancer 2003;3: 721–732
10. Ke Q, Costa M. Hypoxia-inducible factor-1 (HIF-1). Mol Pharmacol 2006;70: 1469–1480
11. Isoe T, Makino Y, Mizumoto K, et al. High glucose activates HIF-1-mediated signal transduction in glomerular mesangial cells through a carbohydrate response element binding protein. Kidney Int 2010;78:48–59
12. Shih SC, Claffey KP. Role of AP-1 and HIF-1 transcription factors in TGF-beta activation of VEGF expression. Growth Factors 2001;19:19–34
13. McMahon S, Charbonneau M, Grandmont S, Richard DE, Dubois CM. Transforming growth factor beta1 induces hypoxia-inducible factor-1 stabilization through selective inhibition of PHD2 expression. J Biol Chem 2006;281:24171–24181
14. Görlach A, Berchner-Pfannschmidt U, Wotzlaw C, et al. Reactive oxygen species modulate HIF-1 mediated PAI-1 expression: involvement of the GTPase Rac1. Thromb Haemost 2003;89:926–935
15. Sudarshan S, Sourbier C, Kong HS, et al. Fumarate hydratase deficiency in renal cancer induces glycolytic addiction and hypoxia-inducible transcription factor 1alpha stabilization by glucose-dependent generation of reactive oxygen species. Mol Cell Biol 2009;29:4080–4090
16. Frede S, Berchner-Pfannschmidt U, Fandrey J. Regulation of hypoxia-inducible factors during inflammation. Methods Enzymol 2007;435:405–419
17. Jung YJ, Isaacs JS, Lee S, Trepel J, Neckers L. IL-1beta-mediated up-regulation of HIF-1alpha via an NFkappaB/COX-2 pathway identifies HIF-1 as a critical link between inflammation and oncogenesis. FASEB J 2003;17:2115–2117
18. Mora-Fernández C, Domínguez-Pimentel V, de Fuentes MM, Górriz JL, Martínez-Castelao A, Navarro-González JF. Diabetic kidney disease: from physiology to therapeutics. J Physiol 2014;592:3997–4012
19. Diebold I, Petry A, Hess J, Görlach A. The NADPH oxidase subunit NOX4 is a new target gene of the hypoxia-inducible factor-1. Mol Biol Cell 2010;21:2087–2096

20. Block K, Gorin Y, Abboud HE. Subcellular localization of Nox4 and regulation in diabetes. Proc Natl Acad Sci U S A 2009;106:14385–14390
21. Gorin Y, Block K, Hernandez J, et al. Nox4 NAD(P)H oxidase mediates hypertrophy and fibronectin expression in the diabetic kidney. J Biol Chem 2005; 280:39616–39626
22. Sun HL, Liu YN, Huang YT, et al. YC-1 inhibits HIF-1 expression in prostate cancer cells: contribution of Akt/NF-kappaB signaling to HIF-1alpha accumulation during hypoxia. Oncogene 2007;26:3941–3951
23. Epstein PN, Overbeek PA, Means AR. Calmodulin-induced early-onset diabetes in transgenic mice. Cell 1989;58:1067–1073
24. Zheng S, Noonan WT, Metreveli NS, et al. Development of late-stage diabetic nephropathy in OVE26 diabetic mice. Diabetes 2004;53:3248–3257
25. Xu J, Huang Y, Li F, Zheng S, Epstein PN. FVB mouse genotype confers susceptibility to OVE26 diabetic albuminuria. Am J Physiol Renal Physiol 2010; 299:F487–F494
26. Eid AA, Gorin Y, Fagg BM, et al. Mechanisms of podocyte injury in diabetes: role of cytochrome P450 and NADPH oxidases. Diabetes 2009;58:1201–1211
27. Eid AA, Ford BM, Bhandary B, et al. Mammalian target of rapamycin regulates Nox4-mediated podocyte depletion in diabetic renal injury. Diabetes 2013; 62:2935–2947
28. Nishikawa T, Edelstein D, Du XL, et al. Normalizing mitochondrial superoxide production blocks three pathways of hyperglycaemic damage. Nature 2000;404:787–790
29. Heilig CW, Concepcion LA, Riser BL, Freytag SO, Zhu M, Cortes P. Overexpression of glucose transporters in rat mesangial cells cultured in a normal glucose milieu mimics the diabetic phenotype. J Clin Invest 1995;96:1802–1814
30. Heilig CW, Liu Y, England RL, et al. D-glucose stimulates mesangial cell GLUT1 expression and basal and IGF-I-sensitive glucose uptake in rat mesangial cells: implications for diabetic nephropathy. Diabetes 1997;46:1030–1039
31. Qian Y, Feldman E, Pennathur S, Kretzler M, Brosius FC 3rd. From fibrosis to sclerosis: mechanisms of glomerulosclerosis in diabetic nephropathy. Diabetes 2008;57:1439–1445
32. Wang Y, Heilig K, Saunders T, et al. Transgenic overexpression of GLUT1 in mouse glomeruli produces renal disease resembling diabetic glomerulosclerosis. Am J Physiol Renal Physiol 2010;299:F99–F111
33. Matoba K, Kawanami D, Okada R, et al. Rho-kinase inhibition prevents the progression of diabetic nephropathy by downregulating hypoxia-inducible factor 1α. Kidney Int 2013;84:545–554
34. Zampell JC, Yan A, Avraham T, Daluvoy S, Weitman ES, Mehrara BJ. HIF-1α coordinates lymphangiogenesis during wound healing and in response to inflammation. FASEB J 2012;26:1027–1039
35. Yan J, Zhou B, Taheri S, Shi H. Differential effects of HIF-1 inhibition by YC-1 on the overall outcome and blood-brain barrier damage in a rat model of ischemic stroke. PLoS One 2011;6:e27798
36. Nordquist L, Friederich-Persson M, Fasching A, et al. Activation of hypoxia-inducible factors prevents diabetic nephropathy. J Am Soc Nephrol 2015;26:328–338
37. Gorin Y, Block K. Nox as a target for diabetic complications. Clin Sci (Lond) 2013;125:361–382
38. Gorin Y, Block K. Nox4 and diabetic nephropathy: with a friend like this, who needs enemies? Free Radic Biol Med 2013;61:130–142
39. Singh DK, Winocour P, Farrington K. Oxidative stress in early diabetic nephropathy: fueling the fire. Nat Rev Endocrinol 2011;7:176–184
40. Lambeth JD, Kawahara T, Diebold B. Regulation of Nox and Duox enzymatic activity and expression. Free Radic Biol Med 2007;43:319–331
41. Heilig C, Zaloga C, Lee M, et al. Immunogold localization of high-affinity glucose transporter isoforms in normal rat kidney. Lab Invest 1995;73:674–684
42. Mogyorósi A, Ziyadeh FN. GLUT1 and TGF-beta: the link between hyperglycaemia and diabetic nephropathy. Nephrol Dial Transplant 1999;14:2827–2829
43. Ricci C, Iacobini C, Oddi G, et al. Role of TGF-beta/GLUT1 axis in susceptibility vs resistance to diabetic glomerulopathy in the Milan rat model. Nephrol Dial Transplant 2006;21:1514–1524
44. Heilig CW, Brosius FC 3rd, Henry DN. Glucose transporters of the glomerulus and the implications for diabetic nephropathy. Kidney Int Suppl 1997;60: S91–S99